Available online at www.sciencedirect.com
ScienceDirect
Trans. Nonferrous Met. Soc. China 23(2013) 2628−2632
Transactions of Nonferrous Metals Society of China
www.tnmsc.cn

Phase evolution and magnetic properties of $Nd_{9.5}Fe_{81}Zr_3B_{6.5}$ nanocomposite magnets

Hong-chao SHENG[1,2,3], Xie-rong ZENG[1,2,3], Chao-xiang JIN[1,2,3], Hai-xia QIAN[1,2,3]

1. Shenzhen Key Laboratory of Special Functional Materials, Shenzhen University, Shenzhen 518060, China;
2. College of Materials Science and Engineering, Shenzhen University, Shenzhen 518060, China;
3. Shenzhen Engineering Laboratory for Advanced Technology of Ceramics, Shenzhen 518060, China

Received 6 August 2012; accepted 10 December 2012

Abstract: Melt-spun $Nd_{9.5}Fe_{81}Zr_3B_{6.5}$ ribbons were prepared by the melt-spinning technique. The phase evolution and magnetic properties were studied by X-ray diffraction, differential scanning calorimetry, transmission electron microscopy observations, and magnetization measurements. It is indicated that melt spinning at different wheel velocities caused the as-quenched ribbons to have distinctive structure. The phase transformation of the ribbons during annealing takes place in two steps: α-Fe transforms from the amorphous phase firstly, followed by formation of $Nd_2Fe_{14}B$ phase. With increasing the initial quenching rate, the microstructure of optimally heat treated ribbons becomes coarser, which results in the weakening of the exchange coupling effect between the hard and soft phase. This leads to drastic deterioration of magnetic properties of annealed ribbons with increasing the initial quenching rate.
Key words: Nd−Fe−B; nanocomposites; Zr addition; magnetic properties

1 Introduction

Nanocomposite magnetic materials consisting of a fine mixture of magnetically hard and soft phases with nanometer size have attracted considerable interest for potential permanent magnet development since they could, by exchange interaction, lead to very high remanence values and potential energy products even with a low content of rare-earth elements [1−3]. However, the experimental value is far smaller than the theoretical value [4−7]. Using a three dimensional modeling, SCHREFL et al [8,9] estimated that the ideal grain size should be approximately 20 nm for the hard phases and 10 nm for the soft phases. However, in real nanocomposite permanent magnets prepared by melt spinning, the grain size is quite large. This is the main reason for the differences in magnetic properties between the practical nanocomposite magnets and the theoretical model [10−13]. Therefore, the refinement of microstructure is expected to be the way to realize the high performance for nanocomposite permanent magnets.

It was reported that the additions of Zr can refine and homogenize the grains, thus enhance exchange coupling interaction between hard and soft magnetic phases and excellent magnetic properties were obtained [14,15]. However, there are no studies on the influence of the initial structure properties of over-quenched precursor phase on the formation, structure, and magnetic properties of the resulting nanocrystalline materials. In this article, we present a systematic study on microstructure evolutions and magnetic properties of as-quenched amorphous and partially crystallized $Nd_{9.5}Fe_{81}Zr_3B_{6.5}$ ribbons during annealing, and clarify how the as-quenched structure influences the crystallization process, the resulting nanocrystalline two-phase structures, and their magnetic properties.

2 Experimental

Alloy ingots with compositions of $Nd_{9.5}Fe_{81}Zr_3B_{6.5}$ were prepared by vacuum induction melting and crushed into small pieces to accommodate the size of the crucible for melt spinning. A quartz nozzle with an orifice of around 0.8 mm in diameter was used and the distance

Foundation item: Projects (51201109, 51001076) supported by the National Natural Science Foundation of China; Project (T201108) supported by Shenzhen Key Laboratory of Special Functional Materials, China
Corresponding author: Xie-rong ZENG; Tel: +86-755-26557459; Fax: +86-755-26536239; E-mail: zengxier@szu.edu.cn
DOI: 10.1016/S1003-6326(13)62777-6

between the orifice and the copper wheel surface was maintained at 3 mm during the melt spinning. Four ribbon samples with composition of $Nd_{9.5}Fe_{81}Zr_3B_{6.5}$ were obtained from the same master alloy by melt spinning on a copper wheel at different peripheral velocities (50, 30, 25, and 20 m/s). The annealing of as-quenched ribbons was carried out in an evacuated quartz tube by soaking the ribbons at different temperatures for 10 min and then cooling them with water. The ribbon samples before or after annealing were characterized by X-ray diffraction (XRD) with Cu K_α radiation, and transmission electron microscopy (TEM). Thermal analysis was employed to characterize the ribbons using a differential scanning calorimeter (DSC) at a heating rate of 20 °C/min. Heating was carried out in flowing purified argon gas during the DSC analysis. The magnetic properties of the ribbons were measured with a vibrating sample magnetometer using a maximum applied field of 2 T.

3 Results and discussion

Figure 1 shows XRD patterns of as-quenched $Nd_{9.5}Fe_{81}Zr_3B_{6.5}$ ribbon samples prepared by melt spinning at different copper wheel velocities. The XRD pattern of ribbon melt spun at 50 m/s shows only amorphous phase. At lower wheel velocities, samples consist of amorphous phase and crystalline phases of both $Nd_2Fe_{14}B$ and α-Fe, and the volume fraction of the amorphous phase increases with increasing quenching rate.

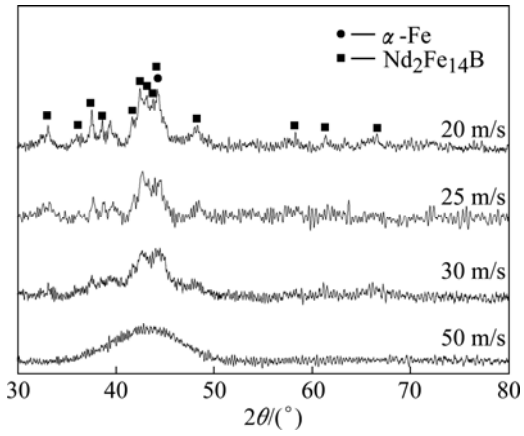

Fig. 1 XTD patterns of $Nd_{9.5}Fe_{81}Zr_3B_{6.5}$ melt-spun at various copper wheel velocities in as-quenched state

In order to study the phase transformation process, isothermal annealing experiments were carried out on ribbons quenched at 50 m/s and 25 m/s. Figure 2 shows the XRD results of as-quenched samples after annealing at different temperatures for 10 min. It is shown that α-Fe phase precipitates firstly from the amorphous phase at 600 °C. It was reported that inter-granular exchange coupling between the hard and soft magnetic phases strengthens significantly, and that the magnetic properties obviously improve by addition of Zr. It was believed that Zr addition can restrain the formation and growth of α-Fe, and result in simultaneous formation of α-Fe and $Nd_2Fe_{14}B$ from the amorphous phase [15]. However, in our studies, the α-Fe phase precipitates firstly. This illuminates that the addition of Zr may inhibit the prior precipitation of α-Fe, but cannot result in simultaneous formation of α-Fe and $Nd_2Fe_{14}B$. For the ribbon annealed at 650 °C, $Nd_2Fe_{14}B$ phase precipitation takes place, and after annealing at 700 °C, α-Fe and $Nd_2Fe_{14}B$ phases are observed.

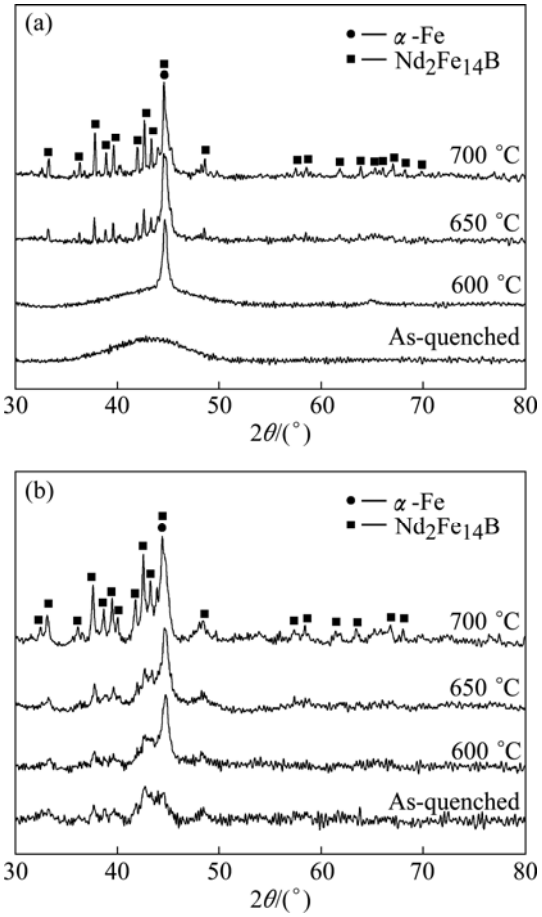

Fig. 2 XRD patterns of $Nd_{9.5}Fe_{81}Zr_3B_{6.5}$ melt-spun at 50 m/s (a), and 25 m/s (b) after annealing at different temperatures

Figure 3 shows the XRD patterns of ribbons obtained at 50, 30, 25, and 20 m/s after thermal treatment at 700 °C for 10 min. It is found that the ribbons consist of hard magnetic $Nd_2Fe_{14}B$ phase and a soft magnetic α-Fe phase, and no additional phases are observed. It can be noticed that the diffraction peaks of the α-Fe and $Nd_2Fe_{14}B$ phases in ribbon spun at 25 m/s and 20 m/s are obviously broadened in comparison with the ribbon spun at 50 m/s and 30 m/s, which implies that the crystalline phases in the as-quenched ribbons decrease the grain size.

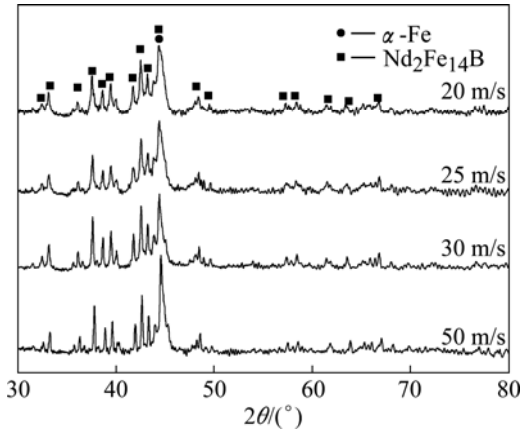

Fig. 3 XRD patterns of $Nd_{9.5}Fe_{81}Zr_3B_{6.5}$ melt-spun at various copper wheel velocities in annealed state

The microstructure of the annealed ribbons was investigated using TEM. Figure 4 shows bright-field TEM micrographs of optically annealed ribbon samples. It can be seen that the grain size of both α-Fe and $Nd_2Fe_{14}B$ phases in the samples decreases significantly with the decrease of initial quenching rate. For annealed ribbons melt-spun at 50 m/s, the grains are nonuniformly distributed with an average grain size of around 70 nm. Large grains with an average grain size of around 50 nm are also present in the microstructure of annealed ribbons melt-spun at 30 m/s. For annealed ribbons melt-spun at 20 m/s and 25 m/s, the grains are uniformly distributed with an average grain size of around 20 nm. The microstructure changes in the annealed samples with increasing initial quenching rate (as indicated by TEM) may be determined by the factor that in the as-quenched ribbons the crystalline phases, which may act as nucleation centers during the crystallization of the amorphous phase, decrease with increasing initial quenching rate. Lack of nucleation sites during the crystallization of highly over-quenched ribbons could lead to a coarse-grained, inhomogeneous microstructure.

Figure 5 shows a wheel speed dependence of the magnetic properties of the samples after annealing at 700 °C for 10 min. It is found that the intrinsic coercivity (H_c) of the annealed ribbons remains almost constant (around 580 kA/m) at the wheel speeds ranging from 20 m/s to 25 m/s, and decreases gradually with the wheel speed. The remanence and energy product have similar tendencies with wheel speed. They reach the maximum value (0.94 T for J_r and 112 kJ/m^3 for $(BH)_{max}$,

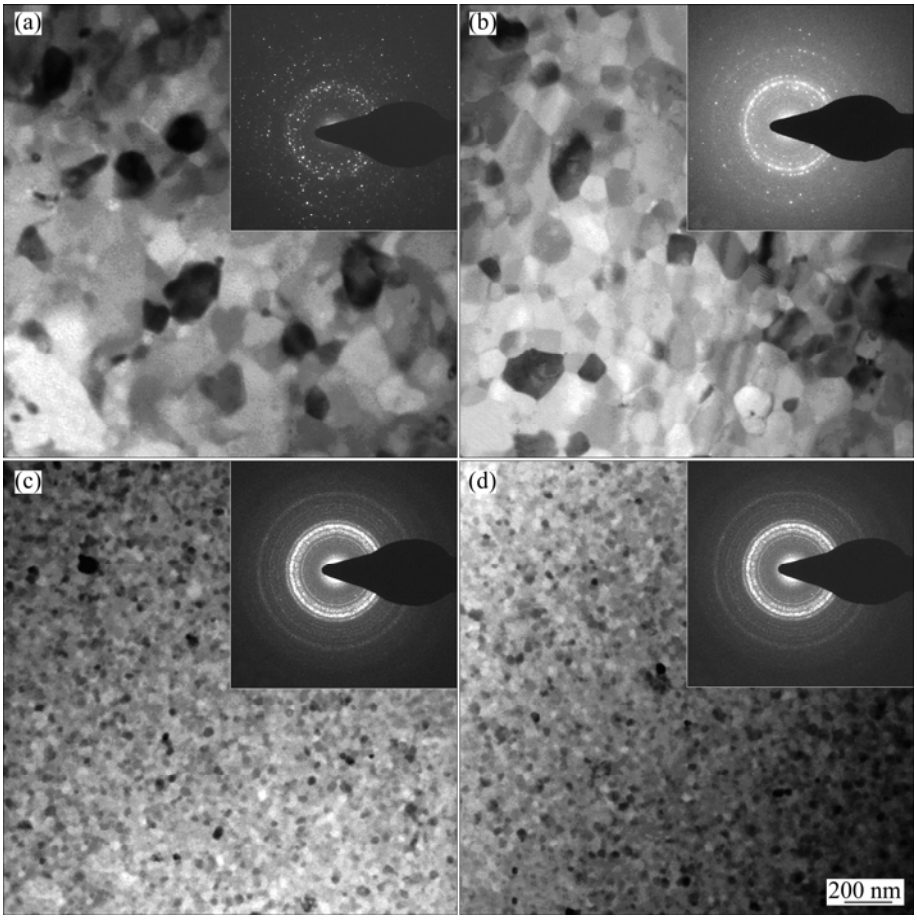

Fig. 4 Bright-field TEM images of ribbons melt-spun at 50 m/s (a), 30 m/s (b), 25 m/s (c) and 20 m/s (d) after annealing at 700 °C for 10 min (The inset is the corresponding selected area diffraction pattern)

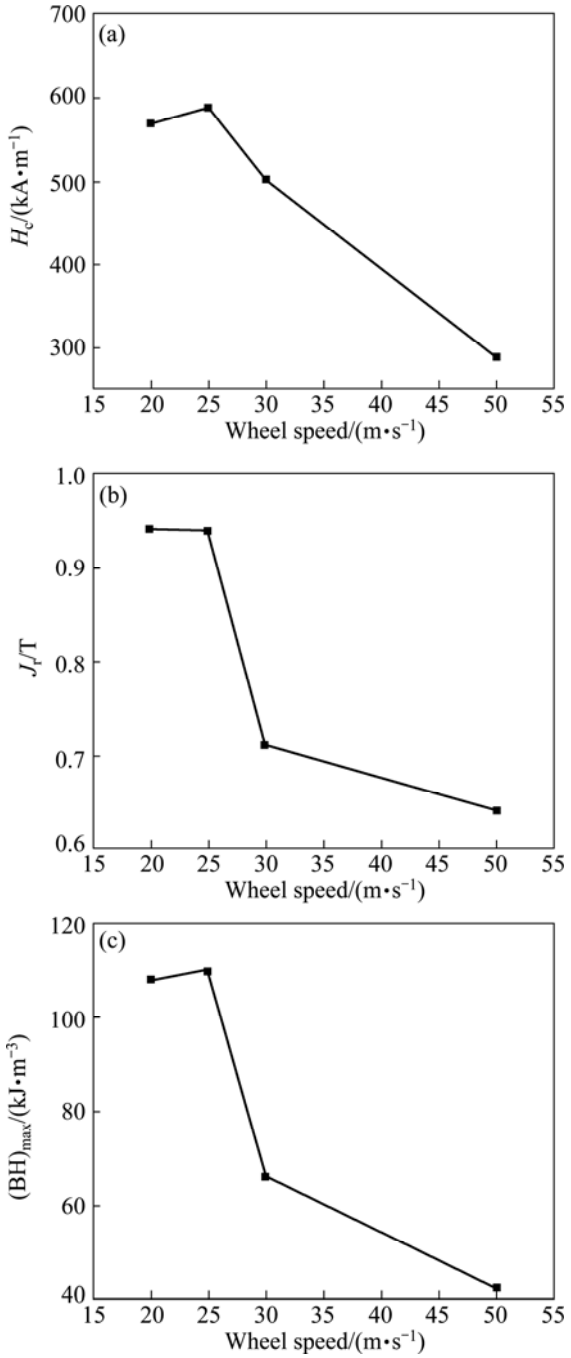

Fig. 5 Dependence of H_c (a), J_r (b), and $(BH)_{max}$ (c) on copper wheel velocities

respectively) at 20 m/s, and remain almost constant at 25 m/s, then the remanence and energy product decrease sharply with further increase of the wheel speed.

Figure 6 presents the demagnetization curves of ribbons after optimal annealing treatment. For the ribbons quenched at 20 m/s and 25 m/s, the demagnetization curves exhibit single-phase magnetic behavior, namely, no two-phase step or kink could be observed. This suggests that in the two samples, hard magnetic grains strongly exchange and are coupled with the neighboring soft grains and the magnetization vectors of hard and soft phases rotate in a cluster feature during the magnetization reversal. Ribbons spun at 30 m/s show a low coercivity, and when the wheel speed increases to 50 m/s, which is greater than the optimum wheel speed, the magnetic properties deteriorate significantly. This is believed to result from the coarser grains which behavior partly or even completely decoupled from the neighboring grains.

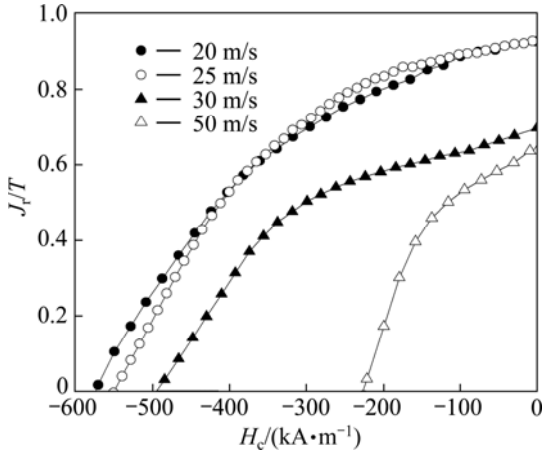

Fig. 6 Demagnetization curves for $Nd_{9.5}Fe_{81}Zr_3B_{6.5}$ melt-spun at various copper wheel velocities after optimal annealing treatment (700 °C, 10 min)

4 Conclusions

1) For all the ribbons, the microstructure after optimal annealing consists of only magnetically hard $Nd_2Fe_{14}B$ phase and soft magnetic α-Fe phase. The phase transformation of the as-quenched ribbons during annealing takes place in two steps: α-Fe transformed from the amorphous phase firstly, followed by formation of $Nd_2Fe_{14}B$ phase.

2) A uniform $Nd_2Fe_{14}B/\alpha$-Fe nanocomposite structure with fine grains can be developed at optimum wheel speed ranging from 20 m/s to 25 m/s. After thermal treatment, the magnetic properties reach a maximum value: H_c=588 kA/m, J_r=0.94 T, $(BH)_{max}$=112 kJ/m^3. In the case of ribbons quenched at higher speeds (>30 m/s), the grains of ribbons after thermal treatment are coarser, resulting from lack of nucleation sites during the crystallization, and the magnetic properties deteriorate significantly, which leads to drastic deterioration of magnetic properties of annealed ribbons.

References

[1] KNELLER E F, HAWIG R. The exchange-spring magnet: A new material principle for permanent [J]. IEEE Trans on Mag, 1991, 27: 3588−3600.

[2] LIU Xin-cai, XIE Ren, PAN Jing. Magnetization arrangement of hard magnetic phases and mechanism of magnetization and reversal magnetization of nano-composite magnets [J]. Transactions of

Nonferrous Metals Society of China, 2009, 19(5): 1131−1145.
[3] WANG Ying, WANG Er-de. Effects of milling and crystallization conditions on microstructure of $Nd_2Fe_{14}B/\alpha$-Fe powder [J]. Transactions of Nonferrous Metals Society of China, 2007, 17(1): 138−142.
[4] YANG C J, PARK E B, HWANG Y S, KIM E C. Enhancement of magnetic properties of $Fe_3B/Nd_2Fe_{14}B$ magnets by the addition of Co [J]. J Magn Magn Mater, 1999, 35: 3328−3331.
[5] SATOSHI H, HIROKAZU K, TOSHIO M. Development of high-coercivity nanocomposite permanent magnets based on Nd_2Fe1_4B and Fe_xB [J]. Journal of Alloys and Compounds, 2006, 408: 260−265.
[6] AKIHISA I, AKIRA T, AKIHIRO M. Hard magnetic properties of nanocrystalline Fe-rich Fe−Nd−B alloys prepared by partial crystallinzation of amorphous phase [J]. Materials Transactions, JIM, 1995, 36: 962−971.
[7] FISCHER R, KRONMULLER H. Static computational micromagnetism of demagnetization processes in nanoscaled permanent magnets [J]. Phys Rev B, 1996, 54: 7284−7294.
[8] SCHREFL T, FISCHER R, FIDLER T. Two- and three-dimensional calculation of remanence enhamcement of rare-earth based composite magnets [J]. J Apple Phys, 1994, 76(10): 7053−7057.
[9] SCHREFL T, FIDLER J, KRONMULLER H. Remanence and coercivity in the isotropic nanocrystalline permanent magnets [J]. Phys Rev B, 1994, 49: 6100−6110.
[10] FIDLER T, FIDLER J, KRONMULLER H. Nucleation field of hard magnetic particles in 2D and 3D micromagnetic calculations [J]. J Magn Magn Mater, 1994, 138: 15−30.
[11] RINTARO I, TOSHIO M, HIROKAZU K, SATOSHI H. High-coercivity nanocomposite permanent magnet based on Nd−Fe−B−Ti−C with Cr addition for high-temperature applications [J]. J Magn Magn Mater, 2007, 312: 410−413.
[12] WANG H, ZHANG Y, JIN Z Q, HADJIPANAYIS G C. Effect of Co substitution on the crystallization behavior and magnetic properties of melt-spun $(Pr,Tb)_2(Fe,Nb,Zr)_{14}B/\alpha$-Fe nanocomposites [J]. J Appl Phys, 2003, 93: 7978−7980.
[13] WANG Zuo-cheng, ZHOU Shou-zeng, QIAO Yi, ZHANG Mao-cai, WEI Run. Phase transformations and magnetic properties of melt-spun $Pr_7Fe_{88}B_5$ ribbons during annealing [J]. J Alloy Comp, 2002, 299: 258−263.
[14] KIM H, CHO S, KIM Y, KIM H, KAPUSTIN G A. Nanocrystalline NdFeB magnets fabricated by a modified hot-working process [J]. J Appl Phy, 2002, 93: 8137−8139.
[15] HIROSAWA S, KANEKIYO H, SHIGEMOTO Y, MURAKAMI K, MIYOSHI T, SHICYA Y. Solidification and crystallization behaviors of $Fe_3B/Nd_2Fe_{14}B$-based nanocomposite permanent-magnet alloys and influence of micro-alloyed Cu, Nb and Zr [J]. J Magn Magn Mate, 2002, 239: 424−430.

$Nd_{9.5}Fe_{81}Zr_3B_{6.5}$ 纳米复相永磁材料的物相演变及磁性能

盛洪超[1,2,3]，曾燮榕[1,2,3]，靳朝相[1,2,3]，钱海霞[1,2,3]

1. 深圳大学 深圳市特种功能材料重点实验室，深圳 518060；
2. 深圳大学 材料学院，深圳 518060；
3. 深圳大学 深圳陶瓷先进技术工程实验室，深圳 518060

摘 要：利用单辊快淬法制备 $Nd_{9.5}Fe_{81}Zr_3B_{6.5}$ 合金条带，采用 X 射线衍射、差式扫描热分析、透射电子显微分析和振动磁强计等分析测试手段，对合金条带的物相演变和磁性能进行研究。结果表明：在不同快淬速度的条件下，合金条带的微观组织结构不同；在热处理过程中，合金的晶化过程分两步完成：α-Fe 首先析出，$Nd_2Fe_{14}B$ 随后析出。随着快淬速度的增大，最佳热处理后合金的晶粒变粗，这使得软磁相和硬磁相之间的交换耦合作用减弱，进而导致合金磁性能的降低。

关键词：钕铁硼；纳米复相；添加 Zr；磁性能

(Edited by Hua YANG)